electronics

MDPI

Article

A Single-Transmitter Multi-Receiver Wireless Power Transfer System with High Coil Misalignment Tolerance and Variable Power Allocation Ratios

Yanting Luo *, Zhuoyue Dai and Yongmin Yang

National Key Laboratory of Equipment State Sensing and Smart Support, College of Intelligence Science and Technology, National University of Defense Technology, Changsha 410073, China; daizhuoyue2019@163.com (Z.D.); yangyongmin@163.com (Y.Y.)
* Correspondence: luoyanting0717@126.com

Abstract: This article proposes a single-transmitter multi-receiver wireless power transfer (STMR-WPT) system, which uses a cross-overlapped bipolar coil as the transmitter and multiple square unipolar coils as the receivers. By using this structure, the magnetic field of the system can be adjusted to accommodate different coil misalignment conditions. In addition, the proposed system uses C-CLCs networks to achieve separate load power allocation. Thus, relay coils, complex multi-frequency transmission channels and multiple independent power supplies can be avoided. A mapping impedance-based circuit model was established to analyze the characteristics of the system, and then a single-frequency power allocation method was presented. Through this method, the STMR-WPT system can achieve load power allocation at any specified ratios under different mutual inductance and load impedance conditions. Finally, an experimental STMR-WPT system was built. The side lengths of the transmitter and receiver coils are 400 mm and 160 mm, respectively. The measurement results indicated that when the lateral or longitudinal coil misalignment varies within the range of 0~200 mm, the coupling coefficient decreases by a maximum of 6% compared to the initial value, and when the angular coil misalignment varies within the range of 0~90 degrees, the coupling coefficient decreases by a maximum of 22% compared to the initial value. In four different power allocation scenarios, the experimental STMR-WPT system successfully achieved the expected power allocation goals.

Keywords: cross-overlapped bipolar transmitter coil; load power allocation; single-transmitter multi-receiver; tolerance for coil misalignment; wireless power transfer

Citation: Luo, Y.; Dai, Z.; Yang, Y. A Single-Transmitter Multi-Receiver Wireless Power Transfer System with High Coil Misalignment Tolerance and Variable Power Allocation Ratios. *Electronics* **2024**, *13*, 3838. https://doi.org/10.3390/electronics13193838

Academic Editor: Fabio Corti

Received: 6 August 2024
Revised: 12 September 2024
Accepted: 25 September 2024
Published: 28 September 2024

1. Introduction

Wireless power transfer (WPT) technology using coupled magnetic resonance has become a research hotspot in recent years due to its high efficiency over medium distances, good flexibility and safety, and the ability to transfer power through non-magnetic materials [1,2]. The single-transmitter single-receiver (STSR) WPT system has been widely studied and successfully applied in fields such as wireless charging for portable devices [3], electric vehicles [4], underwater equipment [5], and implantable medical devices [6]. However, the STSR-WPT system still has some limitations, including that the coupling strength of the system is very sensitive to coil misalignments, and it cannot simultaneously transfer power to multiple load devices [7,8]. Therefore, WPT systems with multiple transmitters or receivers were developed by researchers.

Compared with STSR-WPT systems, WPT systems with multiple transmitters or receivers have some special advantages. The magnetic field distribution of the multi-transmitter single-receiver (MTSR) WPT system can be adjusted by changing the input currents of the transmitter coils. Therefore, it has stronger flexibility than the STSR-WPT

system and can better adapt to coil misalignment [9–12]. The single-transmitter multi-receiver (STMR) WPT system can simultaneously transfer power to multiple receivers through a common transmitter coil [13–15]. The multi-transmitter multi-receiver (MTMR) WPT system has the above advantages, but the system structure is very complex [16,17].

Because the STMR-WPT system has a simpler structure than the MTMR-WPT system and can charge multiple load devices simultaneously, it has attracted a lot of attention. In practical applications, different loads usually have different charging power requirements [18,19]. Therefore, for the STMR-WPT system, one of the key issues that needs to be addressed is how to allocate the power of the transmitter and deliver sufficient power to each receiver. Previous power allocation methods used for the WPT system with multiple receivers mainly included relay coil based methods [20–22] and multi-frequency transmission channel based methods [23–28].

In [20], a relay coil based method was proposed to achieve power allocation for the STMR-WPT system. A one-to-four WPT system was built, which could provide 10 W of power to each receiver. In [21], a multi-relay WPT system was presented, where each relay coil transferred power to an adjacent coil while its local load consumed power. In [22], two power allocation methods were presented for a multi-relay WPT system, including equal power allocation (EPD) and sequential power allocation (SPD). The EPD method allowed each receiver to achieve the same power by adjusting its load resistance, while the SPD method transferred power to the receivers in order of their positions. However, using the relay coil based methods cannot achieve separate load power allocation. If one of the relay coils loses resonance, its subsequent coils will be affected.

In [23], the frequency bifurcation phenomenon was utilized to achieve power allocation for multiple loads and reduce the cross interference between different power transmission channels. However, the frequency bifurcation phenomenon only occurs in the over-coupling region of the transmitter and receiver coils. The article in Ref. [24] introduced a dual-frequency compatible STMR-WPT system, in which the power injected into the transmitter coil included two frequency components. The receivers were optimally designed to have different resonant frequencies and could pick up power through frequency selective resonance. But this system only had two receivers.

In order to achieve separate power allocation for more receivers, an LCL-LC composited compensation topology was developed in [25]. By using this topology, multiple transmission channels with different resonant frequencies can be constructed. In [26], a multi-frequency STMR-WPT system was designed, which could allocate the source power to different receivers with arbitrary load power requirements. The article in Ref. [27] proposed a STMR-WPT system that features a three-phase high-frequency inverter and multiple delta-type transmitting tanks, which can simultaneously transfer power to multiple receivers at different frequencies. Although the previous methods [25–28] can achieve separate power allocation for multiple receivers, they need to construct complex multi-frequency transmission channels and use independent power supplies with different frequencies, which will obviously increase the system size and cost.

In some application scenarios, the position of the load device may change, leading to misalignment between the transmitter and receiver coils. Coil misalignment can significantly reduce the efficiency of the STMR-WPT system and affect the load power allocation results [29]. To address the issues caused by coil movement, the article in Ref. [30] proposed a T/Y-maze-based WPT system, in which the transmitter coil array consists of eight rectangular resonators. When the receiver coil moves along the transmitter coil array, this WPT system can achieve uniform wireless power transmission. The article in Ref. [31] presented an eight-folded star-shaped transmitter coil structure. Two layers of transmitter coils were designed as square and overlapping at 45 degrees angles to each other. This transmitter coil has good tolerance for coil angular misalignment. Even when the receiver has an angular coil misalignment of 90 degrees, the receiver can still obtain power from the transmitter.

In [32], an asymmetric flat cross-shaped solenoid coupling coil with high lateral misalignment tolerance was developed, which can provide more free charging positions for

the receivers. The article in Ref. [33] proposed a 3D omnidirectional coil structure, in which the current amplitude and phase of the transmitter could be adjusted to achieve magnetic field shaping and maximum efficiency tracking. In [34], A 3D open box-shaped transmitter was presented, which could generate magnetic fields in all directions. Despite the lateral and angular coil misalignments, the receiver could still obtain sufficient power from the transmitter. However, this 3D transmitter has a complex structure and a large dimension.

To overcome the limitations of traditional STMR-WPT systems, this article proposes a STMR-WPT system with high coil misalignment tolerance and variable power allocation ratios. A mapping impedance-based circuit model was established to analyze the characteristics of the system, and then a single-frequency power allocation method was presented. Finally, an experimental STMR-WPT system was built and the feasibility of the proposed method was verified by experiments. The main contributions of this article include:

(1) A coupling coil structure with high misalignment tolerance was developed, which includes a cross-overlapped bipolar transmitter coil, multiple square unipolar receiver coils and a switch. By changing the switch state, the magnetic field of the transmitter coil can be adjusted to accommodate different misalignments of the receiver coils. In the experiment, the side lengths of the transmitter and receiver coils are 400 mm and 160 mm. When the lateral or longitudinal coil misalignment varies within the range of 0~200 mm, the coupling coefficient decreases by a maximum of 6% compared to the initial value. When the angular coil misalignment varies within the range of 0~90 degrees, the coupling coefficient decreases by a maximum of 22% compared to the initial value. Therefore, the proposed coil structure allows the receivers to have more flexible charging positions.

(2) A single-frequency power allocation method is proposed for the STMR-WPT system. The C-CLCs networks are constructed to achieve separate load power allocation for the receivers. Thus, relay coils, complex multi-frequency transmission channels and multiple independent power supplies can be avoided, which is beneficial for reducing the system size and cost. Through the proposed method, the STMR-WPT system can operate in single-frequency mode and achieve power allocation at any specified ratios under different mutual inductance and load impedance conditions.

2. Overview of the STMR-WPT System

A traditional STMR-WPT system is shown in Figure 1, which includes a planar-spiral transmitter coil, multiple planar-spiral receiver coils, loads, resonance capacitors and independent power supplies with different frequencies.

Although the STMR-WPT system shown in Figure 1 can charge multiple receivers simultaneously, there are still some limitations:

(1) The performance of this STMR-WPT system is very sensitive to coil misalignments. As shown in Figure 1, if the receiver coil-1 has a lateral misalignment, its coupling coefficient with the transmitter coil will deviate from the optimal value, which may lead to a significant decrease in the system efficiency. In addition, as the angular misalignment of the receiver coil-2 increases, its coupling coefficient with the transmitter coil will rapidly decrease. When the angular misalignment reaches 90 degrees, the coupling coefficient will be very low. Even if the frequency of the power supply can be adjusted, it is difficult for the receiver coil-2 to obtain sufficient power from the transmitter coil.

(2) In order to achieve separate load power allocation, this STMR-WPT system requires the use of complex multi-frequency transmission channels and independent power supplies with different frequencies, which will significantly increase the system size and cost. Moreover, due to some system parameters such as coil inductance and load impedance changing with the source frequency, using multi-frequency mode will complicate the system response and increase the difficulty of system design.

To overcome these limitations, this article proposes an improved STMR-WPT system structure. As shown in Figure 2a, it mainly includes a single-frequency power supply, a

cross-overlapped bipolar transmitter coil, a switch, multiple square unipolar receiver coils, loads and C-CLCs networks.

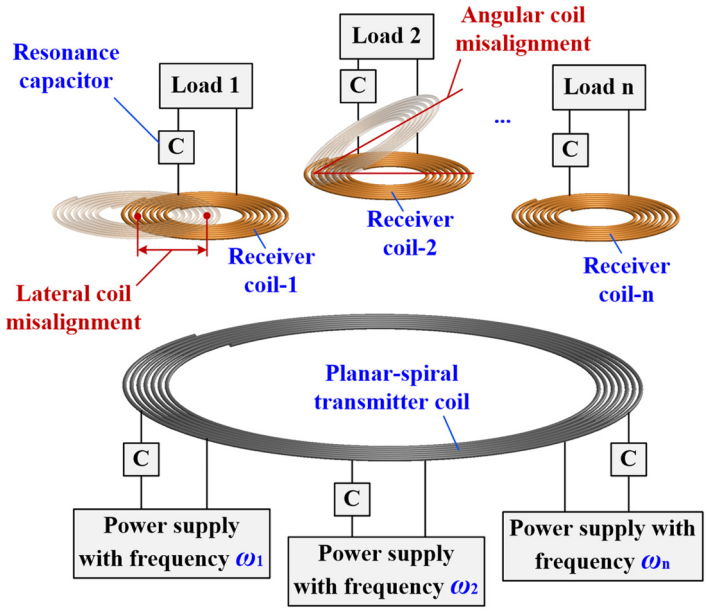

Figure 1. Structure of a traditional STMR-WPT system.

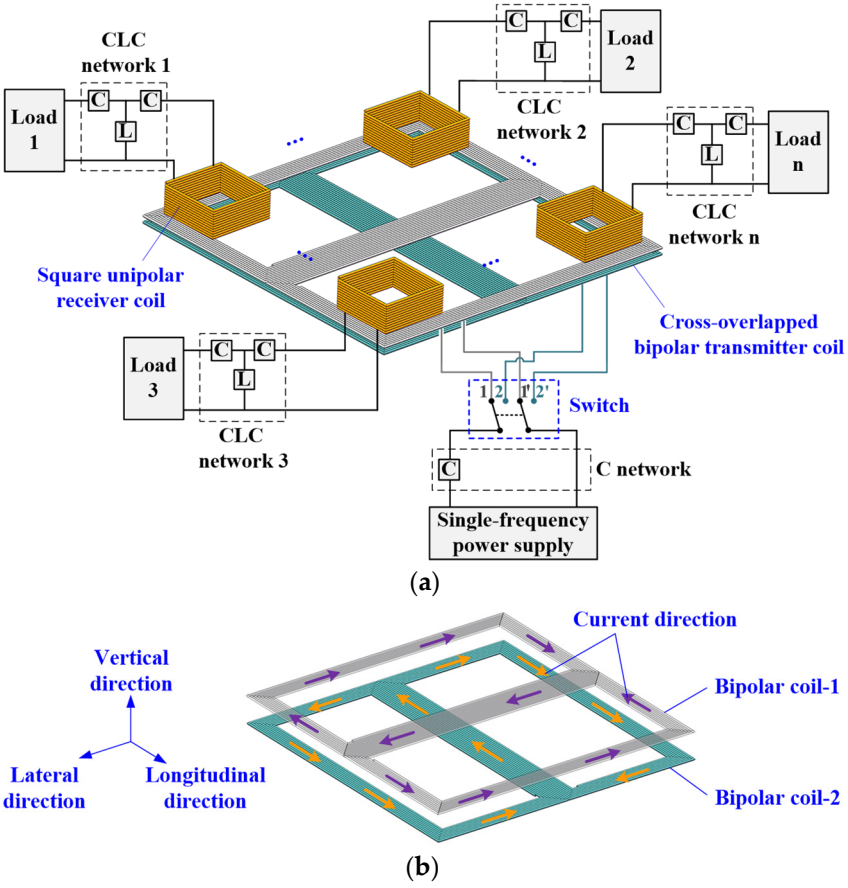

Figure 2. Schematic diagram of the proposed STMR-WPT system. (**a**) Structure of the STMR-WPT system. (**b**) Structure of the cross-overlapped bipolar transmitter coil.

The cross-overlapped bipolar transmitter coil consists of two square bipolar coils, labeled as bipolar coil-1 and bipolar coil-2. The two bipolar coils are orthogonally overlapped

together, as shown in Figure 2b. The square unipolar receiver coils are placed on one pole of the bipolar transmitter coil. The side length of the receiver coil is designed to be less than half of the side length of the transmitter coil.

The switch is used to change the connection of the bipolar coils. As shown in Figure 2a, when the switch is turned to the 1-1′ position, the bipolar coil-1 is connected to the transmitter circuit of the system. When the switch is turned to the 2-2′ position, the bipolar coil-2 is connected to the transmitter circuit of the system. By changing the switch state, the magnetic field of the cross-overlapped bipolar transmitter coil can be adjusted to adapt to the position changes of the receiver coil. Activating only one bipolar coil at the same time is beneficial for reducing leakage flux and increase the system efficiency.

In addition, the proposed STMR-WPT system uses C-CLCs networks to achieve separate load power allocation, rather than using relay coils or constructing complex multi-frequency transmission channels. The C-CLCs networks consist of variable capacitors and inductors. Their values can be adjusted according the actual power allocation demands. Specifically, the CLC networks in the receiver circuits are used to transform the load impedances to the optimal values and ensure that the receiver coils meet the resonance conditions. The C network in the transmitter circuit is used to adjust the imaginary part of the circuit impedance and ensure that the transmitter coil meets the resonance condition. By using C-CLCs networks, the STMR-WPT system can operate in single-frequency mode and achieve the expected power allocation goals.

3. Modeling and Analysis of the STMR-WPT System

3.1. Simulation Analysis of the Coupling Coils

In some WPT scenarios, such as wireless charging for mobile electronic devices, the position of the receiver may change. In addition to parallel movement, the receiver may also rotate. Therefore, coil misalignments that occur in the WPT system can be classified into lateral, longitudinal, and angular misalignments. To analyze the performance of the proposed coupling coils under different misalignment conditions, simulation analysis is carried out using ANSYS Maxwell 16.0. The simulation steps are as follows: Firstly, determine the coil size and material, and establish a simulation model of the coil. Secondly, set simulation parameters, including excitation current and frequency. Thirdly, start the simulation calculation. When the simulation calculation is completed, the magnetic field distribution of the coil and the coupling coefficient between the coils can be obtained.

A simulation model is first established. As shown in Figure 3a, the cross-overlapped bipolar transmitter coil model consists of two square bipolar coils made of copper wire with a diameter of 2.8 mm. The side length of the bipolar coil is set to 400 mm, and the number of turns of the bipolar coil is eight. The excitation current and frequency are set to 100 A and 500 kHz, respectively. Because the two square bipolar coils are orthogonally overlapped together, the coupling coefficient between them is very small. Through simulation, it can be obtained that the value of the coupling coefficient is 1.2832×10^{-4}, as shown in Figure 3b. Therefore, the mutual inductance effect between the two bipolar coils can be ignored.

The magnetic field distribution of the cross-overlapped bipolar transmitter coil is also analyzed. Figure 3c,d show the simulated magnetic field distribution of the cross-overlapped bipolar transmitter coil when the switch is turned to the 1-1′ and 2-2′ positions, respectively. It can be observed that the magnetic field of the cross-overlapped bipolar transmitter coil can be adjusted by changing the switch state.

The square unipolar receiver coil is also made of copper wire with a diameter of 2.8 mm. The side length of the receiver coil is set to 160 mm, and the number of turns of the receiver coil is 12. As shown in Figure 4, the receiver coil is arranged at an initial position on one pole of the transmitter coil, where the transmitter and receiver coils are considered aligned in the lateral, longitudinal and angular directions. The vertical distance between the coils is set to 25 mm.

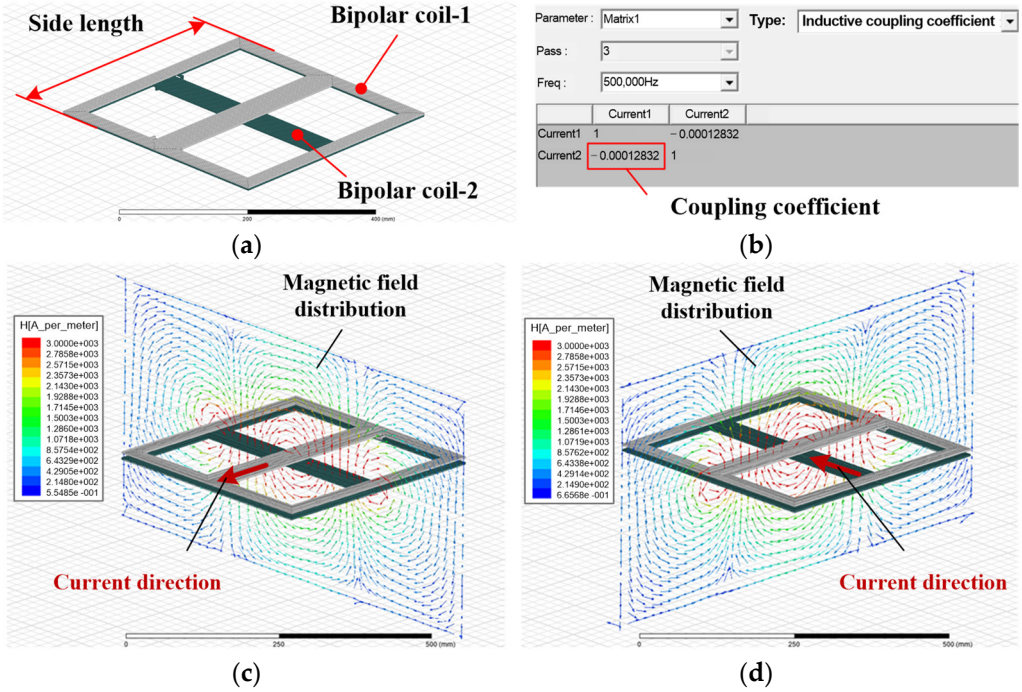

Figure 3. Simulation of the cross-overlapped bipolar transmitter coil. (**a**) Simulation model. (**b**) Simulation result of the coupling coefficient between bipolar coil-1 and coil-2. (**c**) Magnetic field distribution of the transmitter coil when the switch is turned to the 1-1′ position. (**d**) Magnetic field distribution of the transmitter coil when the switch is turned to the 2-2′ position.

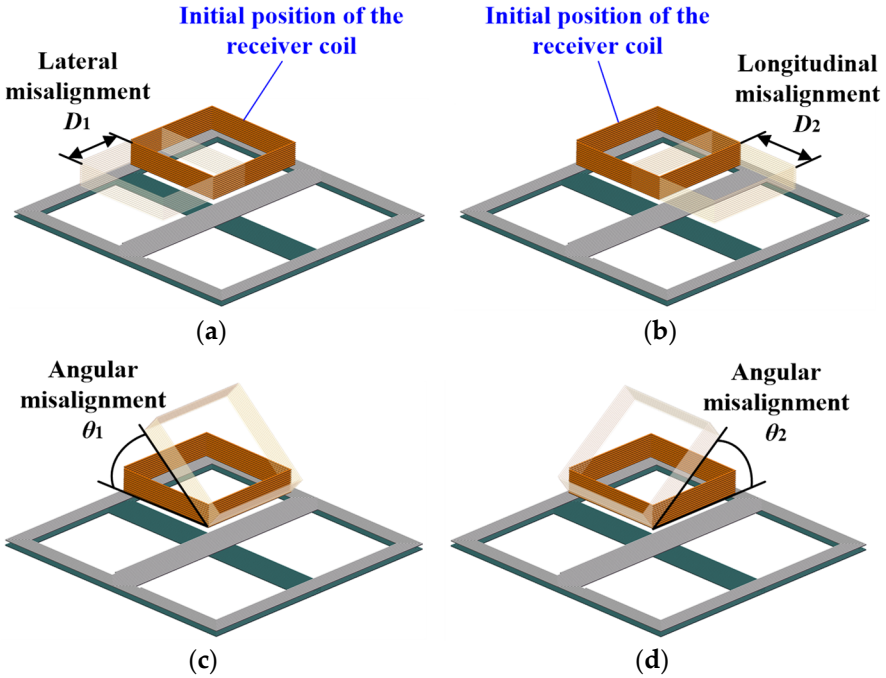

Figure 4. Schematic diagram of the transmitter and receiver coils with (**a**) lateral coil misalignment D_1; (**b**) longitudinal coil misalignment D_2; (**c**) angular coil misalignment θ_1; (**d**) angular coil misalignment θ_2.

To simulate the lateral and longitudinal coil misalignments, the receiver coil is moved along the lateral or longitudinal direction, as shown in Figure 4a,b. To simulate the angular coil misalignment, the receiver coil is rotated around the lateral or longitudinal direction,

as shown in Figure 4c,d. The coupling coefficients between the transmitter coil and the receiver coil under different coil misalignment conditions are analyzed.

Figure 5a–d show the simulated coupling coefficients under the conditions of lateral misalignment D_1, longitudinal misalignment D_2, angular misalignment θ_1 and angular misalignment θ_2, respectively, where K_{1r} is the simulated coupling coefficient between the bipolar coil-1 and the receiver coil, and K_{2r} is the simulated coupling coefficient between the bipolar coil-2 and the receiver coil.

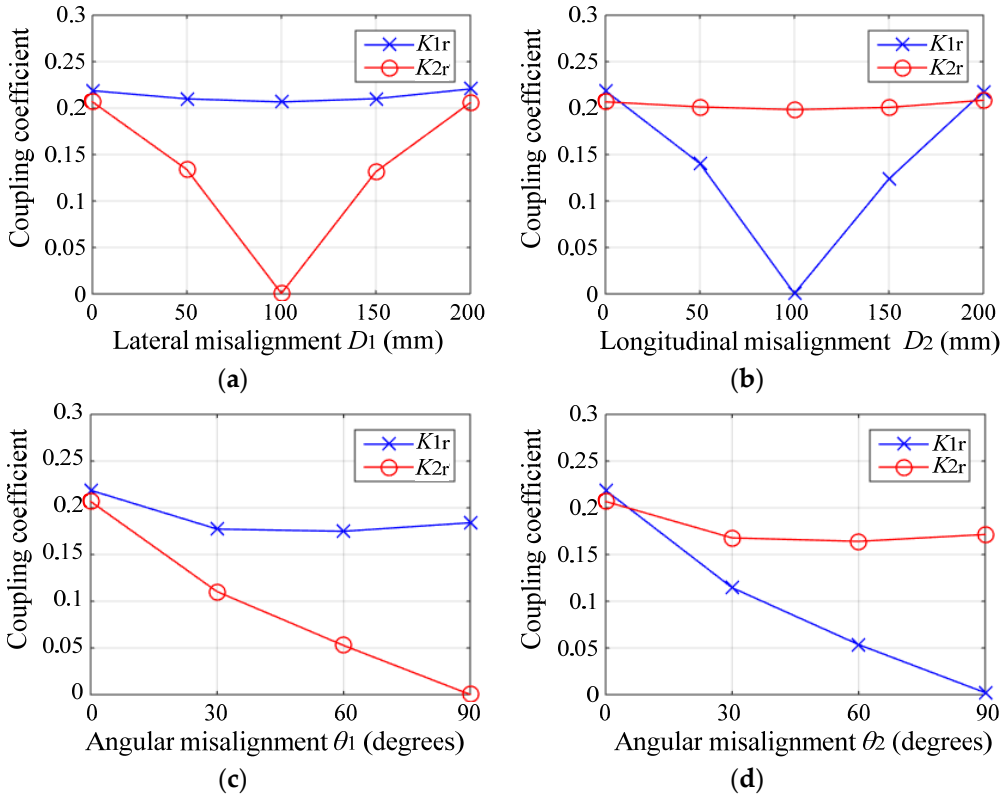

Figure 5. Simulated coupling coefficients between the cross-overlapped bipolar transmitter coil and the square unipolar receiver coil with (**a**) lateral coil misalignment D_1; (**b**) longitudinal coil misalignment D_2; (**c**) angular coil misalignment θ_1; (**d**) angular coil misalignment θ_2.

From Figure 5a, it can be seen that as the lateral coil misalignment D_1 increases, the coupling coefficient K_{1r} remains stable, but K_{2r} changes dramatically. Therefore, by turning the switch to the 1-1′ position, the cross-overlapped bipolar transmitter coil can better adapt to the lateral misalignment of the receiver coil. Similarly, it can be seen from Figure 5b that as the longitudinal coil misalignment D_2 increases, K_{1r} changes greatly, but K_{2r} remains stable. Therefore, by turning the switch to the 2-2′ position, the cross-overlapped bipolar transmitter coil can better adapt to the longitudinal misalignment of the receiver coil.

From Figure 5c, it can be observed that as the angular coil misalignment θ_1 increases, the coupling coefficient K_{1r} slightly changes; however, K_{2r} rapidly drops to zero. Therefore, when the switch is turned to the 1-1′ position, the cross-overlapped bipolar transmitter coil has better tolerance for the angular coil misalignment θ_1. Figure 5d illustrates that as θ_2 increases, K_{1r} rapidly drops to zero, but K_{2r} slightly changes. Therefore, when the switch is turned to the 2-2′ position, the cross-overlapped bipolar transmitter coil has better tolerance for the angular coil misalignment θ_2.

The simulation results show that the proposed coupling coil structure has good tolerances for coil misalignments. By changing the switch state, even if the transmitter and receiver coils are misaligned, the coupling coefficient does not change significantly.

According to the previous studies [29–34], the coupling coefficient changes caused by coil misalignments will significantly affect the load power ratios of the STMR-WPT system. Therefore, using the proposed coupling coil structure is beneficial for stabilizing the coupling coefficient and achieving the expected power allocation goal.

3.2. Circuit Analysis of the STMR-WPT System

When the number of the receiver coils $n = 3$, the STMR-WPT system can be equivalent to the circuit model shown in Figure 6, where U_s, ω and R_s are the voltage, frequency and internal resistance of the power supply. C_{ts} is the series capacitance in the transmitter circuit and the inductances of bipolar coil-1 and bipolar coil-2 are L_1 and L_2, respectively. To simplify the analysis, it is assumed that $L_1 = L_2 = L_t$. Because only one bipolar coil is connected to the transmitter circuit at the same time, the equivalent inductance of the transmitter coil is L_t.

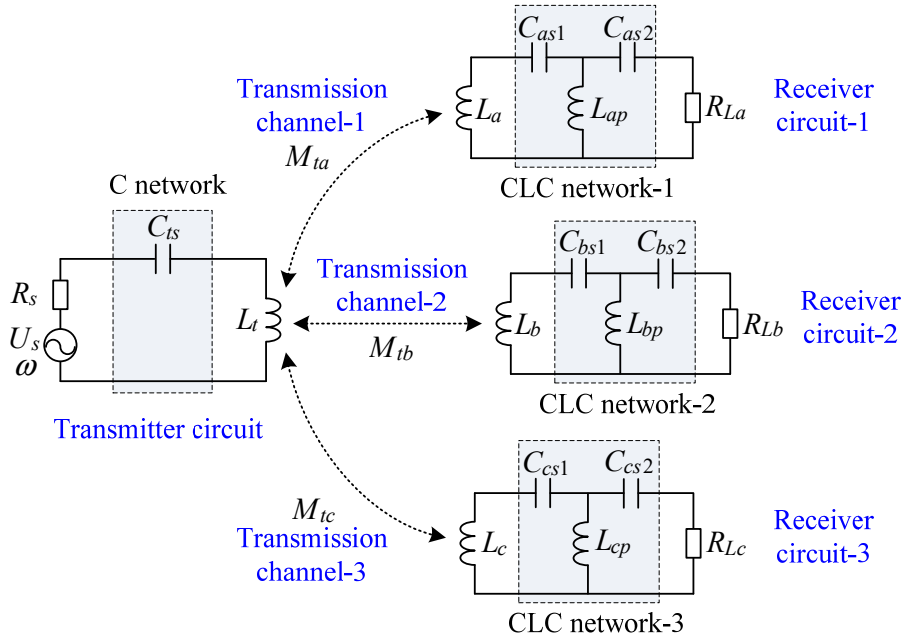

Figure 6. Equivalent circuit of the proposed STMR-WPT system.

In Figure 6, L_a, L_b and L_c are the inductances of the receiver coil-1, coil-2 and coil-3, respectively. L_{ap}, C_{as1} and C_{as2} represent the parallel inductance, series capacitance-1 and series capacitance-2 of the CLC network-1. L_{bp}, C_{bs1} and C_{bs2} represent the parallel inductance, series capacitance-1 and series capacitance-2 of the CLC network-2. L_{cp}, C_{cs1} and C_{cs2} represent the parallel inductance, series capacitance-1 and series capacitance-2 of the CLC network-3. M_{ta}, M_{tb} and M_{tc} are the mutual inductances between the transmitter coil and the receiver coils. Because the receiver coils are placed in positions where they are decoupled from each other, the mutual inductances between the receiver coils are ignored. R_{La}, R_{Lb} and R_{Lc} are, respectively, the load resistances in the receiver circuit-1, circuit-2 and circuit-3.

The STMR-WPT system includes three power transmission channels. In order to analyze the power flow of the system and obtain the transmission characteristics of each channel, the circuit model shown in Figure 6 is further equivalent to the mapping impedance-based circuit model shown in Figure 7, where Z_a, Z_b and Z_c represent the mapping impedances from the receiver circuit-1, receiver circuit-2 and receiver circuit-3 to the transmitter circuit. I_t represents the current in the transmitter circuit. I_a, I_b and I_c represent the currents in the receiver circuit-1, receiver circuit-2 and receiver circuit-3. P_s is the source output power. P_a, P_b and P_c are the power obtained by the receiver circuit-1,

receiver circuit-2 and receiver circuit-3. The meanings of the other system parameters in Figure 7 are the same as those in Figure 6.

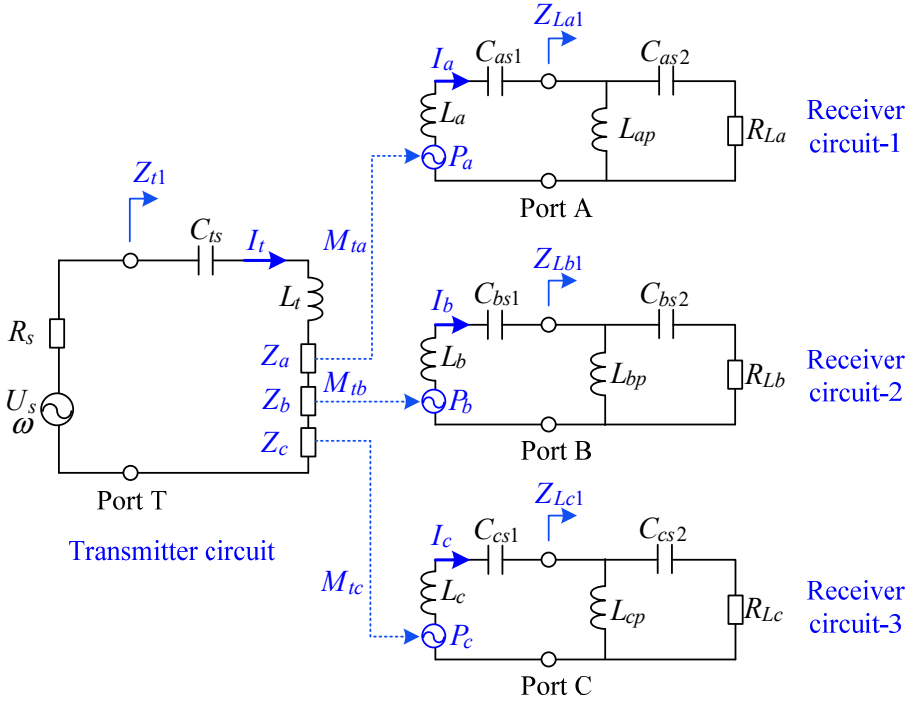

Figure 7. Mapping impedance-based model of the STMR-WPT system.

Based on the mutual inductance theory, the mapping impedances Z_a, Z_b and Z_c can be calculated as:

$$\begin{cases} Z_a = \frac{j\omega M_{ta} I_a}{I_t} = \frac{\omega^2 {M_{ta}}^2}{Z_{La1}+j\omega L_a+1/j\omega C_{as1}} \\ Z_b = \frac{j\omega M_{tb} I_b}{I_t} = \frac{\omega^2 {M_{tb}}^2}{Z_{Lb1}+j\omega L_b+1/j\omega C_{bs1}} \\ Z_c = \frac{j\omega M_{tc} I_c}{I_t} = \frac{\omega^2 {M_{tc}}^2}{Z_{Lc1}+j\omega L_c+1/j\omega C_{cs1}} \end{cases} \tag{1}$$

where Z_{La1} is the input impedance at Port A, Z_{Lb1} is the input impedance at Port B, and Z_{Lc1} is the input impedance at Port C. According to the circuit structure, it is prone to obtain the following:

$$\begin{cases} Z_{La1} = \frac{j\omega L_{ap}(R_{La}+1/j\omega C_{as2})}{R_{La}+j\omega L_{ap}+1/j\omega C_{as2}} \\ Z_{Lb1} = \frac{j\omega L_{bp}(R_{Lb}+1/j\omega C_{bs2})}{R_{Lb}+j\omega L_{bp}+1/j\omega C_{bs2}} \\ Z_{Lc1} = \frac{j\omega L_{cp}(R_{Lc}+1/j\omega C_{cs2})}{R_{Lc}+j\omega L_{cp}+1/j\omega C_{cs2}} \end{cases} \tag{2}$$

The current in the transmitter circuit can be calculated as:

$$I_t = \frac{U_s}{R_s + j\omega L_t + 1/j\omega C_t + Z_a + Z_b + Z_c} \tag{3}$$

Then, the apparent power obtained by the receiver circuits can be found:

$$\begin{cases} P_a = \left| {I_t}^2 Z_a \right| \\ P_b = \left| {I_t}^2 Z_b \right| \\ P_c = \left| {I_t}^2 Z_c \right| \end{cases} \tag{4}$$

The active power absorbed by the loads can be calculated as:

$$\begin{cases} P_{La} = |I_t|^2 \mathrm{Re}(Z_a) \\ P_{Lb} = |I_t|^2 \mathrm{Re}(Z_b) \\ P_{Lc} = |I_t|^2 \mathrm{Re}(Z_c) \end{cases} \tag{5}$$

where $\mathrm{Re}(Z_a)$, $\mathrm{Re}(Z_b)$ and $\mathrm{Re}(Z_c)$ represent the real parts of Z_a, Z_b and Z_c, respectively.

The power transfer efficiency (PTE) is often used to evaluate the performance of the WPT system, which is defined as the ratio of the load power to the actual output power of the source. However, even in high PTE situations, the load power may still be low, as the source output power will vary with the load impedance. To solve this problem, this article selected the power gain (PG) to evaluate the STMR-WPT system. The PGs of the three power transmission channels are defined as:

$$\begin{cases} G_a = \frac{P_{La}}{P_{s-\max}} \\ G_b = \frac{P_{Lb}}{P_{s-\max}} \\ G_c = \frac{P_{Lc}}{P_{s-\max}} \end{cases} \tag{6}$$

where $P_{s-\max}$ represents the maximum source output power, which can be calculated as:

$$P_{s-\max} = \frac{{U_s}^2}{4R_s} \tag{7}$$

From (7), it can be seen that when the source voltage U_s and internal resistance R_s are given, $P_{s-\max}$ is determined and does not change with the load impedance. Therefore, if the PG of the WPT system reaches its maximum value, both the PTE and the load power will be maximized.

By substituting (5) and (7) into (6), it can be derived that:

$$\begin{cases} G_a = \frac{4R_s \mathrm{Re}(Z_a)}{|R_s + j\omega L_t + 1/j\omega C_t + Z_a + Z_b + Z_c|^2} \\ G_b = \frac{4R_s \mathrm{Re}(Z_b)}{|R_s + j\omega L_t + 1/j\omega C_t + Z_a + Z_b + Z_c|^2} \\ G_c = \frac{4R_s \mathrm{Re}(Z_c)}{|R_s + j\omega L_t + 1/j\omega C_t + Z_a + Z_b + Z_c|^2} \end{cases} \tag{8}$$

From (5) and (8), it can be seen that the load powers P_{La}, P_{Lb} and P_{Lc}, and PGs G_a, G_b and G_c are proportional to the real part of the mapping impedances $\mathrm{Re}(Z_a)$, $\mathrm{Re}(Z_b)$ and $\mathrm{Re}(Z_c)$. In addition, due to the fact that the total load power $P_{total} = P_{La} + P_{Lb} + P_{Lc}$ should be smaller than the maximum source output power, the total PG of the system $G_{total} = G_a + G_b + G_c$ is less than or equal to 1.

4. Single-Frequency Power Allocation Method for the STMR-WPT System

4.1. Power Allocation Conditions

For the STMR-WPT system, how to allocate the power of the transmitter and provide sufficient power to each receiver is a key problem that needs to be solved.

From (5), it can be seen that the load powers P_{La}, P_{Lb} and P_{Lc} are proportional to the real parts of the mapping impedances $\mathrm{Re}(Z_a)$, $\mathrm{Re}(Z_b)$ and $\mathrm{Re}(Z_c)$, respectively. Therefore, if the power allocation goal is $P_{La} = \gamma_b P_{Lb} = \gamma_c P_{Lc}$, where γ_b and γ_c are the power allocation ratios, the following power allocation conditions should be satisfied:

$$\mathrm{Re}(Z_a) = \gamma_b \mathrm{Re}(Z_b) = \gamma_c \mathrm{Re}(Z_c) \tag{9}$$

Based on (1) and (2), it can be seen that Z_a, Z_b and Z_c are related to the CLC networks of the receiver circuits. By adjusting the series capacitances and parallel inductances in

the CLC networks, the real parts of the mapping impedances can be transformed into the desired ratios. Then, the expected power allocation goal can be achieved.

To simplify the analysis, the CLC networks are assumed to meet the following resonance conditions:

$$\begin{cases} \omega L_{ap} - 1/\omega C_{as2} = 0 \\ \omega L_{bp} - 1/\omega C_{bs2} = 0 \\ \omega L_{cp} - 1/\omega C_{cs2} = 0 \\ \omega (L_a + L_{ap}) - 1/\omega C_{as1} = 0 \\ \omega (L_b + L_{bp}) - 1/\omega C_{bs1} = 0 \\ \omega (L_c + L_{cp}) - 1/\omega C_{cs1} = 0 \end{cases} \tag{10}$$

By substituting (10) into (1) and (2), the mapping impedances can be simplified as:

$$\begin{cases} Z_a = \frac{{M_{ta}}^2 R_{La}}{{L_{ap}}^2} \\ Z_b = \frac{{M_{tb}}^2 R_{Lb}}{{L_{bp}}^2} \\ Z_c = \frac{{M_{tc}}^2 R_{Lc}}{{L_{cp}}^2} \end{cases} \tag{11}$$

Based on (11), it can be seen that when (10) is satisfied, the mapping impedances Z_a, Z_b and Z_c only have the real parts. If the mutual inductances M_{ta}, M_{tb} and M_{tc} and the load resistances R_{La}, R_{Lb} and R_{Lc} are given, the mapping impedances are only determined by the parallel inductances L_{ap}, L_{bp} and L_{cp} in the CLC networks.

By substituting (11) into (9), the desired ratios of the parallel inductances can be obtained:

$$\begin{cases} L_{bp} = \frac{M_{tb}}{M_{ta}} \sqrt{\frac{\gamma_b R_{Lb}}{R_{La}}} \times L_{ap} \\ L_{cp} = \frac{M_{tc}}{M_{ta}} \sqrt{\frac{\gamma_c R_{Lc}}{R_{La}}} \times L_{ap} \end{cases} \tag{12}$$

By substituting (12) into (10), the desired values of the series capacitances in the CLC networks can also be found:

$$\begin{cases} C_{as1} = \frac{1}{\omega^2 (L_a + L_{ap})} \\ C_{bs1} = \frac{M_{ta}}{\omega^2 (M_{ta} L_b + M_{tb} L_{ap} \sqrt{\gamma_b R_{Lb} / R_{La}})} \\ C_{cs1} = \frac{M_{ta}}{\omega^2 (M_{ta} L_c + M_{tc} L_{ap} \sqrt{\gamma_c R_{Lc} / R_{La}})} \\ C_{as2} = \frac{1}{\omega^2 L_{ap}} \\ C_{bs2} = \frac{M_{ta}}{\omega^2 M_{tb} L_{ap} \sqrt{\gamma_b R_{Lb} / R_{La}}} \\ C_{cs2} = \frac{M_{ta}}{\omega^2 M_{tc} L_{ap} \sqrt{\gamma_c R_{Lc} / R_{La}}} \end{cases} \tag{13}$$

Based on the above analysis, if the parameters of the CLC networks satisfy (12) and (13), the expected power allocation goal $P_{La} = \gamma_b P_{Lb} = \gamma_c P_{Lc}$ can be achieved.

4.2. Impedance Matching Conditions

In practical applications, because the internal resistance of the power supply consumes a portion of the source power, the actual source output power may not be optimal. As a result, even if the expected power allocation goal $P_{La} = \gamma_b P_{Lb} = \gamma_c P_{Lc}$ is achieved, the total PG of the STMR-WPT system may still be low. Thus, the receivers cannot obtain sufficient power from the transmitter. To address this issue, the impedance matching conditions of the STMR-WPT system are proposed as a supplement to the power allocation conditions.

According to the maximum power transfer theorem, the total PG of the STMR-WPT system can be maximized when the following impedance matching conditions are met:

$$\mathrm{Re}(Z_{t1}) = R_s \text{ and } \mathrm{Im}(Z_{t1}) = 0 \tag{14}$$

where Z_{t1} is the total input impedance at Port T of the transmitter circuit, as shown in Figure 7. $\mathrm{Re}(Z_{t1})$ and $\mathrm{Im}(Z_{t1})$ are the real part and imaginary part of Z_{t1}.

Based on the circuit structure, it is prone to obtain as follows:

$$Z_{t1} = j\omega L_t + \frac{1}{j\omega C_{ts}} + Z_a + Z_b + Z_c \tag{15}$$

When the power allocation conditions in (12) and (13) are satisfied, the total input impedance Z_{t1} can be written as:

$$Z_{t1} = (1 + 1/\gamma_b + 1/\gamma_c)\frac{{M_{ta}}^2 R_{La}}{{L_{ap}}^2} + j(\omega L_t - \frac{1}{\omega C_{ts}}) \tag{16}$$

By substituting (16) into (14), it can be derived that:

$$\begin{cases} L_{ap} = M_{ta}\sqrt{\frac{(1+1/\gamma_b+1/\gamma_c)R_{La}}{R_s}} \\ C_{ts} = \frac{1}{\omega^2 L_t} \end{cases} \tag{17}$$

4.3. Power Allocation Method

Based on the above analysis, when the power allocation conditions in (9) and the impedance matching conditions in (14) are satisfied simultaneously, the STMR-WPT system can achieve the expected power allocation goal while obtaining the maximum total PG. Therefore, a single-frequency power allocation method was proposed for the STMR-WPT system, as shown in Figure 8. The main steps include:

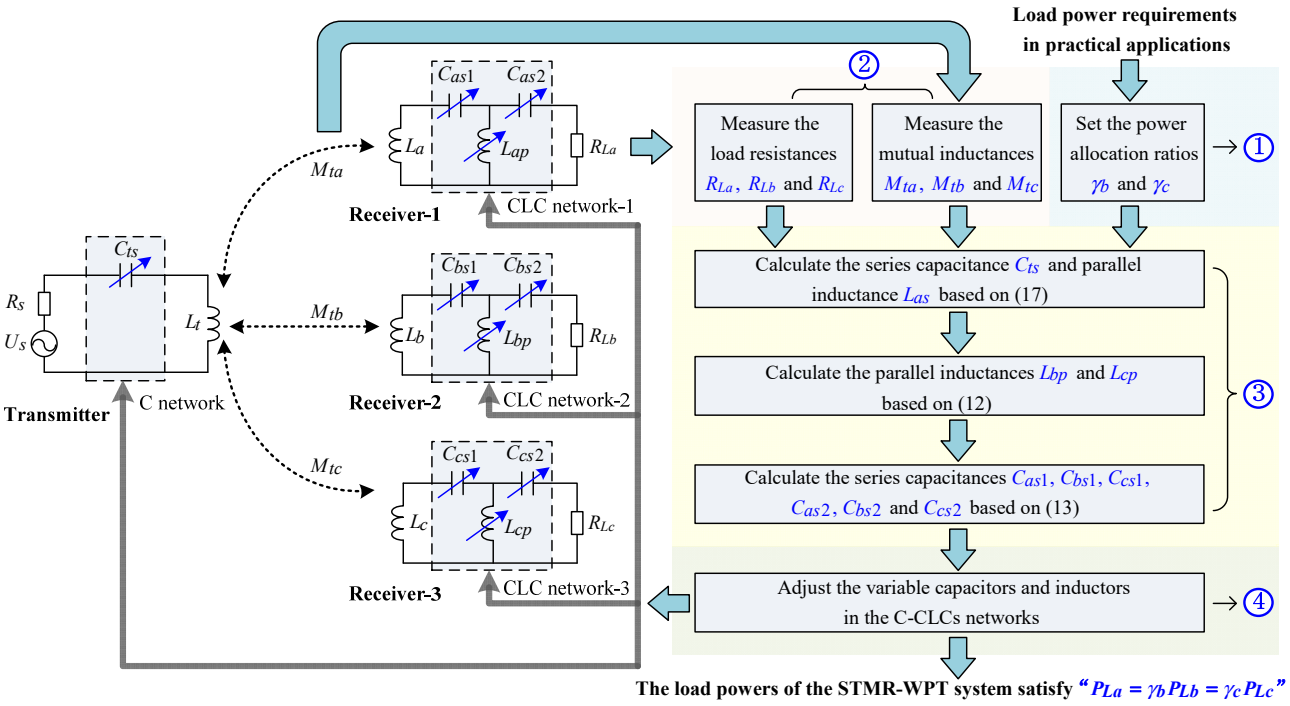

Figure 8. Schematic diagram of the proposed power allocation method.

Step 1: Set the power allocation goal $P_{La} = \gamma_b P_{Lb} = \gamma_c P_{Lc}$. The power allocation ratios γ_b and γ_c are given based on actual application requirements.

Step 2: Measure the load resistances R_{La}, R_{Lb} and R_{Lc} and the mutual inductances M_{ta}, M_{tb} and M_{tc}.

Step 3: Calculate the optimal parameters of the C-CLCs networks. The desired values of the parallel inductance L_{ap} and series capacitance C_{ts} are calculated using (17), the

desired values of the parallel inductances L_{bp} and L_{cp} are calculated using (12), and the desired values of the series capacitances C_{as1}, C_{bs1}, C_{cs1}, C_{as2}, C_{bs2} and C_{cs2} are calculated using (13).

Step 4: Adjust the variable capacitors and inductors in the C-CLCs networks to the desired values obtained in Step 3.

Through the above steps, the STMR-WPT system can be designed to meet $P_{La} = \gamma_b P_{Lb} = \gamma_c P_{Lc}$. The total PG of the system can also be maximized.

The proposed power allocation method has the following advantages:

(1) The C-CLCs networks are constructed to achieve separate power allocation for multiple receivers. Thus, the relay coils, complex multi-frequency transmission channels and independent power supplies with different frequencies can be avoided, which helps to reduce the system size and cost. Through this method, the STMR-WPT system can operate in single-frequency mode and achieve load power allocation at any specified ratios under different mutual inductance and load impedance conditions.

(2) In addition to power allocation, the C-CLCs networks are also used to achieve impedance matching for the STMR-WPT system. By doing so, the total PG of the system can be maximized, which is beneficial for improving the utilization of the power supply and ensuring that the receiver can obtain sufficient load power.

4.4. Numerical Simulations

To show the effectiveness of the proposed single-frequency power allocation method, numerical simulations were conducted on the STMR-WPT system. Considering that the coupling strengths and loads of different receivers may vary in practical situations, the mutual inductances between the transmitter and the receiver-1, receiver-2 and receiver-3 were set to 8 μH, 10 μH and 12 μH, respectively. The load resistances of the receiver-1, receiver-2 and receiver-3 were set to 10 Ω, 50 Ω and 100 Ω, respectively. Table 1 lists the parameters of the STMR-WPT system used for the simulation.

Table 1. Parameters of the STMR-WPT System Used for Simulation.

Parameters	Values
Resonance frequency f	500 kHz
Source internal resistance R_s	50 Ω
Load resistances $R_{La1}/R_{Lb1}/R_{Lc1}$	10/50/100 Ω
Transmitter coil inductance L_t	65 μH
Receiver coil inductances $L_a/L_b/L_c$	45 μH
Mutual inductances $M_{ta}/M_{tb}/M_{tc}$	8/10/12 μH

In practical applications, different loads usually have different charging power requirements. The power allocation ratios of the proposed STMR-WPT system can be set arbitrarily. Table 2 presents four sets of power allocation ratios to simulate different charging scenarios. Based on the proposed power allocation method, the desired values of the C-CLCs networks can be obtained, as listed in Table 3.

Table 2. Power Allocation Ratios in Different Scenarios.

Parameters	Scenario 1	Scenario 2	Scenario 3	Scenario 4
γ_b	1.5	1	0.5	100
γ_c	3	1	100	100

(1) Mapping Impedances and Total Input Impedance of the STMR-WPT System

After obtaining the desired values of the C-CLCs networks, the mapping impedances from the receiver circuits to the transmitter circuit can be calculated using (1), and the total input impedance at Port T of the transmitter circuit can be analyzed using (16).

Table 3. Desired Values of the C-CLCs Networks.

Parameters	Scenario 1	Scenario 2	Scenario 3	Scenario 4
C_{ts}(nF)	1.6	1.6	1.6	1.6
L_{ap}(μH)	5.1	6.2	6.2	3.6
L_{bp}(μH)	17.3	17.3	12.3	101.0
L_{cp}(μH)	41.6	29.4	294.4	171.4
C_{as1}(nF)	2.0	2.0	2.0	2.1
C_{bs1}(nF)	1.6	1.6	1.8	0.7
C_{cs1}(nF)	1.2	1.4	0.3	0.5
C_{as2}(nF)	20.0	16.4	16.3	28.0
C_{bs2}(nF)	5.8	5.8	8.3	1.0
C_{cs2}(nF)	2.4	3.4	0.3	0.6

Figure 9a shows the simulated mapping impedances Z_a, Z_b and Z_c and the total input impedance Z_{t1} in scenario-1, where the power allocation ratios are $\gamma_b = 1.5$ and $\gamma_c = 3$. It can be observed from Figure 9a that at the resonance frequency point 500 kHz, the real parts of the mapping impedances are $\mathrm{Re}(Z_a) = 25\ \Omega$, $\mathrm{Re}(Z_b) = 16.7\ \Omega$ and $\mathrm{Re}(Z_c) = 8.3\ \Omega$. Therefore, the power allocation condition $\mathrm{Re}(Z_a) = 1.5\mathrm{Re}(Z_b) = 3\mathrm{Re}(Z_c)$ can be satisfied. In addition, it can be seen from Figure 9a that at 500 kHz, the real part of the total input impedance $\mathrm{Re}(Z_{t1}) = 50\ \Omega$ and the imaginary part of the total input impedance $\mathrm{Im}(Z_{t1}) = 0\ \Omega$. Thus, the impedance matching conditions $\mathrm{Re}(Z_{t1}) = R_s$ and $\mathrm{Im}(Z_{t1}) = 0\ \Omega$ can also be achieved at the resonance frequency point.

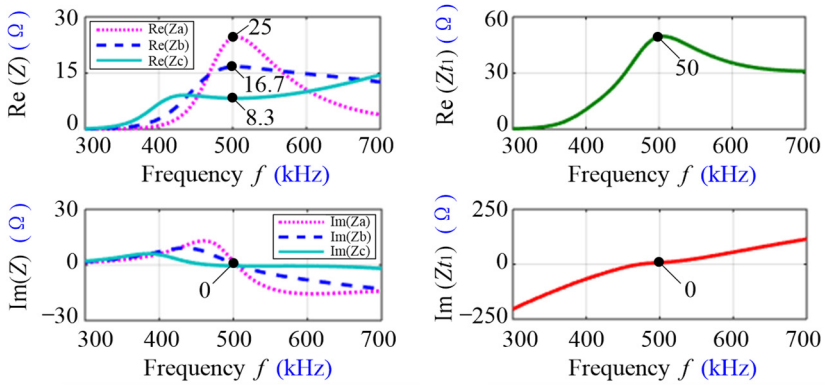

(**a**)

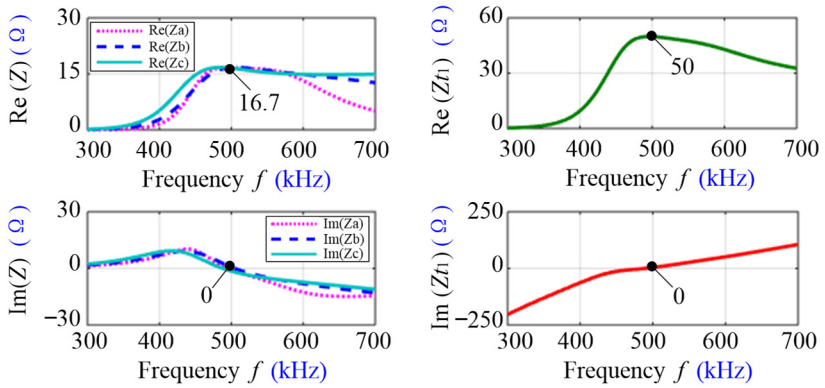

(**b**)

Figure 9. *Cont.*

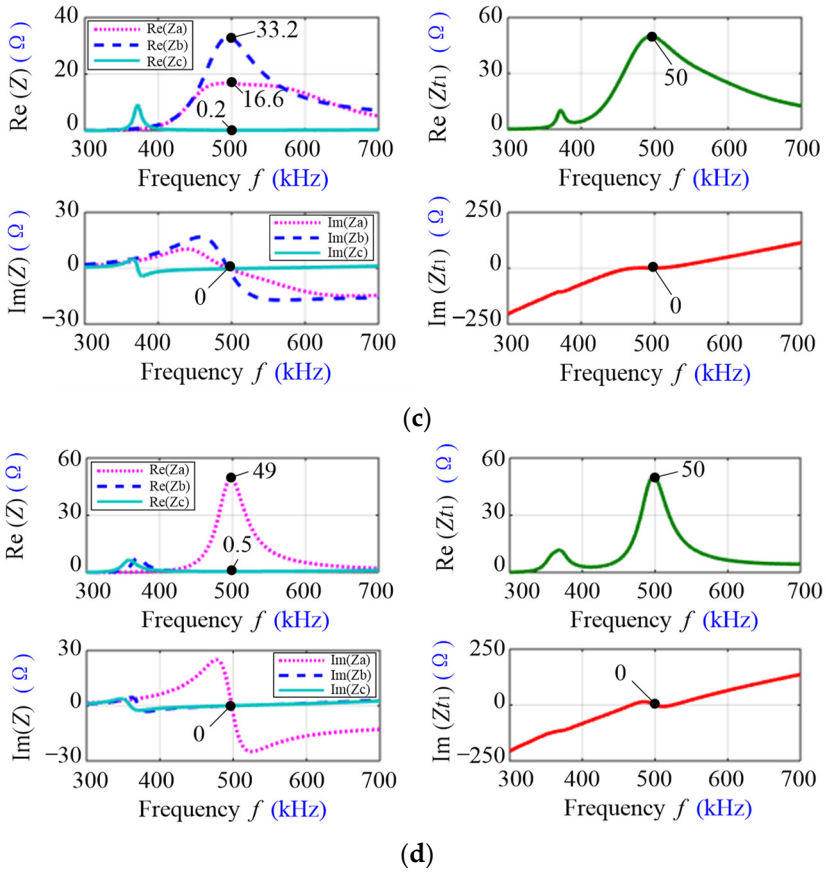

Figure 9. Simulation results of the mapping impedances and total input impedance in (**a**) scenario-1; (**b**) scenario-2; (**c**) scenario-3; (**d**) scenario-4.

Figure 9b–d respectively show the simulated results of the mapping impedances Z_a, Z_b and Z_c and the total input impedance Z_{t1} in power allocation scenario-2 ($\gamma_b = \gamma_c = 1$), scenario-3 ($\gamma_b = 0.5$, $\gamma_c = 100$) and scenario-4 ($\gamma_b = 100$, $\gamma_c = 100$). It can also be seen that the mapping impedances of the system meet the power allocation conditions $\mathrm{Re}(Z_a) = \gamma_b \mathrm{Re}(Z_b) = \gamma_c \mathrm{Re}(Z_c)$ at the resonance frequency point 500 kHz, and the total input impedance of the system satisfies the impedance matching conditions $\mathrm{Re}(Z_{t1}) = R_s$ and $\mathrm{Im}(Z_{t1}) = 0\Omega$ at 500 kHz.

The simulation results show that by using the proposed method, the STMR-WPT system can be adjusted to meet the power allocation conditions and impedance matching conditions at the resonance frequency point.

(2) PGs of the STMR-WPT System

According to the desired values of the C-CLCs networks in Table 3, the PGs of the STMR-WPT system in different power allocation scenarios can be calculated using (8). Figure 10a–d, respectively, show the PGs of the system in scenario-1, scenario-2, scenario-3 and scenario-4.

From Figure 10a, it can be seen that the PGs at 500 kHz are $G_a = 0.5$, $G_b = 0.33$ and $G_c = 0.17$. Therefore, the power transmitted to R_{La} is 1.5 times as much as that transmitted to R_{Lb}, and three times as much as that transmitted to R_{Lc} in scenario-1. It can be observed from Figure 10b that the PGs at the frequency of 500 kHz are $G_a = G_b = G_c = 0.33$. Thus, in scenario-2, the power transmitted to R_{La}, R_{Lb} and R_{Lc} will be the same.

From Figure 10c, it can be observed that the PGs at 500 kHz are $G_a = 0.33$, $G_b = 0.66$ and $G_c = 0.01$. Therefore, in scenario-3, the power transmitted to R_{Lb} is twice as much as that transmitted to R_{La}, and the power obtained by R_{Lc} will be very low. Figure 10d shows that the PGs at 500 kHz are $G_a = 0.98$, $G_b = 0.01$ and $G_c = 0.01$. In scenario-4, most of

the source output power will be transmitted to R_{La}. The powers obtained by R_{Lb} and R_{Lc} will be very low. In addition, it can be seen from Figure 10 that in all four scenarios, the total PG of the system $G_{total} = G_a + G_b + G_c \approx 1$.

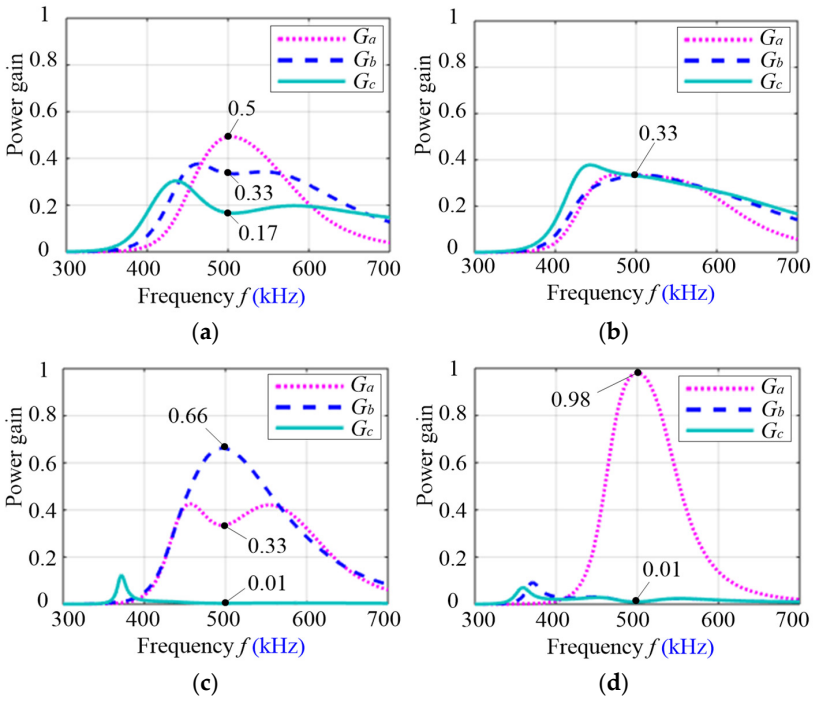

Figure 10. Simulation results of PGs in (**a**) scenario-1; (**b**) scenario-2; (**c**) scenario-3; (**d**) scenario-4.

The simulation results show that through the proposed method, the STMR-WPT system can achieve load power allocation at any specified ratios under different mutual inductance and load impedance conditions. At the same time, the total PG of the STMR-WPT system can be maximized.

In addition, the proposed power allocation method is not limited to the above four scenarios. When the mutual inductance or load impedance changes, the curves in Figures 9 and 10 may change. However, using the method shown in Figure 8, the STMR-WPT system can still meet the power allocation conditions and impedance matching conditions at the resonance frequency point.

5. Experimental Verification

5.1. Measurement of the Mutual Inductances

The performance of the proposed coupling coil structure was verified through experiments. Because the transmitter and receiver coils are both air-core coils, the main power loss of the coils is copper loss. In order to reduce the resistance of the coil at high frequency, the transmitter and receiver coils were wound using 0.1 mm × 400 strands Litz wires. The cross-overlapped bipolar transmitter coil included two bipolar coils with a side length of 400 mm and eight turns. The measured self-inductances of the bipolar coil-1 and bipolar coil-2 were 66.3 μH and 65.4 μH, respectively. The side length of the square unipolar receiver coil was 160 mm, and the number of turns of the receiver coil was 12. The measured inductance of the receiver coil was 44.1 μH.

The coupling performance between the cross-overlapped bipolar transmitter coil and the receiver coil was analyzed under different coil misalignment conditions. As shown in Figure 11, four kinds of coil misalignments were considered in the experiment, including the lateral coil misalignment D_1, longitudinal coil misalignment D_2, angular coil misalignment around the lateral direction θ_1, and angular coil misalignment around the longitudinal direction θ_2.

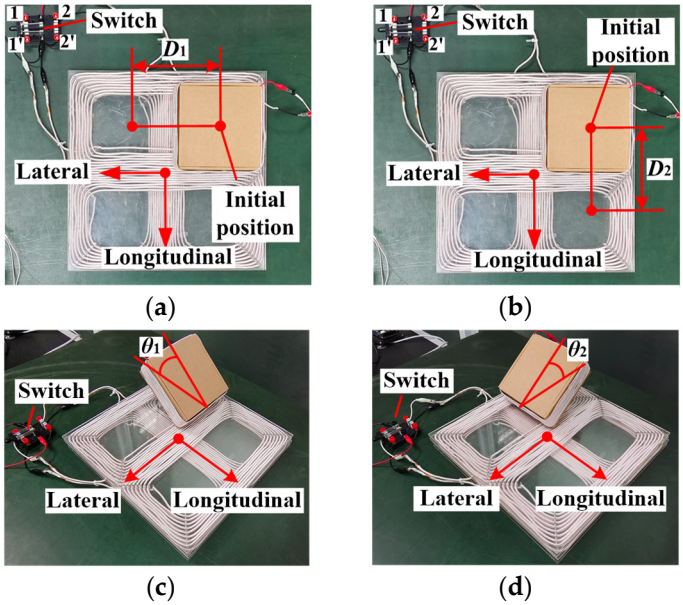

Figure 11. Cross-overlapped bipolar transmitter coil and square unipolar receiver coil with (**a**) lateral coil misalignment D_1; (**b**) longitudinal coil misalignment D_2; (**c**) angular coil misalignment θ_1; (**d**) angular coil misalignment θ_2.

A switch was used to change the connection of the cross-overlapped bipolar transmitter coil. According to the analysis in Part A of Section 3, the magnetic field of the cross-overlapped bipolar transmitter coil can be adjusted to accommodate different coil misalignment conditions. When the switch is turned to the 1-1′ position, the bipolar coil-1 is connected to the transmitter circuit of the system, and the cross-overlapped bipolar transmitter coil can better adapt to the lateral misalignment D_1 and angular misalignment θ_1. When the switch is turned to the 2-2′ position, the bipolar coil-2 is connected to the transmitter circuit of the system, and the cross-overlapped bipolar transmitter coil can better adapt to the longitudinal misalignment D_2 and angular misalignment θ_2.

A high precision impedance analyzer Agilent 4294A was used to measure the mutual inductance between the transmitter and receiver coils. The measurement steps were as follows: Firstly, the transmitter and receiver coils were connected in series, as shown in Figure 12a. The total coil inductance (L_1) was measured using the impedance analyzer. Secondly, the transmitter and receiver coils were connected in series in the opposite direction, as shown in Figure 12b. The total coil inductance (L_2) was measured using the impedance analyzer. Thirdly, the mutual inductance between the coils (M) was calculated by:

$$M = \frac{L_1 - L_2}{4} \tag{18}$$

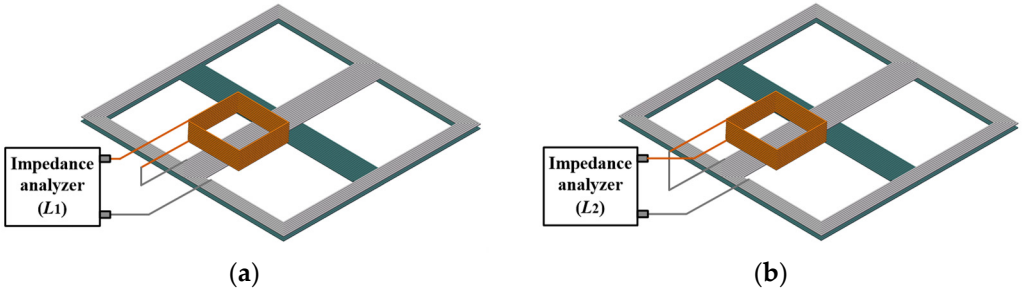

Figure 12. Schematic diagram of the mutual inductance measurement. (**a**) Measurement of the total coil inductance L_1; (**b**) Measurement of the total coil inductance L_2.

The measurement results of the mutual inductance under different coil misalignment conditions are listed in Table 4.

Table 4. Measurement results of the mutual inductance.

Coil Misalignment Condition		Mutual Inductance
Lateral coil misalignment D_1	0 mm	11.30 μH
	50 mm	11.84 μH
	100 mm	11.63 μH
	150 mm	11.57 μH
	200 mm	10.92 μH
Longitudinal coil misalignment D_2	0 mm	10.74 μH
	50 mm	10.85 μH
	100 mm	10.79 μH
	150 mm	10.53 μH
	200 mm	10.10 μH
Angular coil misalignment θ_1	0°	11.30 μH
	30°	9.35 μH
	60°	9.14 μH
	90°	10.38 μH
Angular coil misalignment θ_2	0°	10.74 μH
	30°	8.38 μH
	60°	8.65 μH
	90°	9.51 μH

After obtaining the mutual inductances, the coupling coefficient between the transmitter and receiver coils can be calculated by:

$$k = \frac{M}{\sqrt{L_t L_r}} \tag{19}$$

where L_t is the measured inductance of the transmitter coil and L_r is the measured inductance of the receiver coil.

Figure 13 shows the variations of the coupling coefficient under different coil misalignment conditions. From Figure 13a,b, it can be seen that when the lateral or longitudinal coil misalignment varies within the range of 0~200 mm, the coupling coefficient decreases by a maximum of 6% compared to the initial value. From Figure 13c,d, it can be observed that when the angular coil misalignment varies within the range of 0~90 degrees, the coupling coefficient decreases by a maximum of 22% compared to the initial value.

The measurement results indicate that the proposed coupling coil structure has good tolerances for lateral, longitudinal and angular coil misalignments. Using the proposed coupling coil structure is beneficial for maintaining the coupling strength of the coils and achieving the expected load power allocation goals for the STMR-WPT system.

The reasons for the difference between the experimental values of the coupling coefficient in Figure 13 and the simulated values of the coupling coefficient in Figure 5 include: Firstly, the methods for measuring the coupling coefficient are different. In the simulation, the values of the coupling coefficient were obtained using ANSYS Maxwell software. In the experiment, the measurement method of the coupling coefficient is shown in Figure 12, where only one bipolar coil was connected to the receiver coil at the same time. Therefore, only one coupling coefficient was measured and plotted in Figure 13. Secondly, the parameters of the simulation model are not exactly the same as those of the experimental

prototype. For example, there is a slight deviation in the inner length and self-inductance of the transmitter coil, which is difficult to avoid in the experiments.

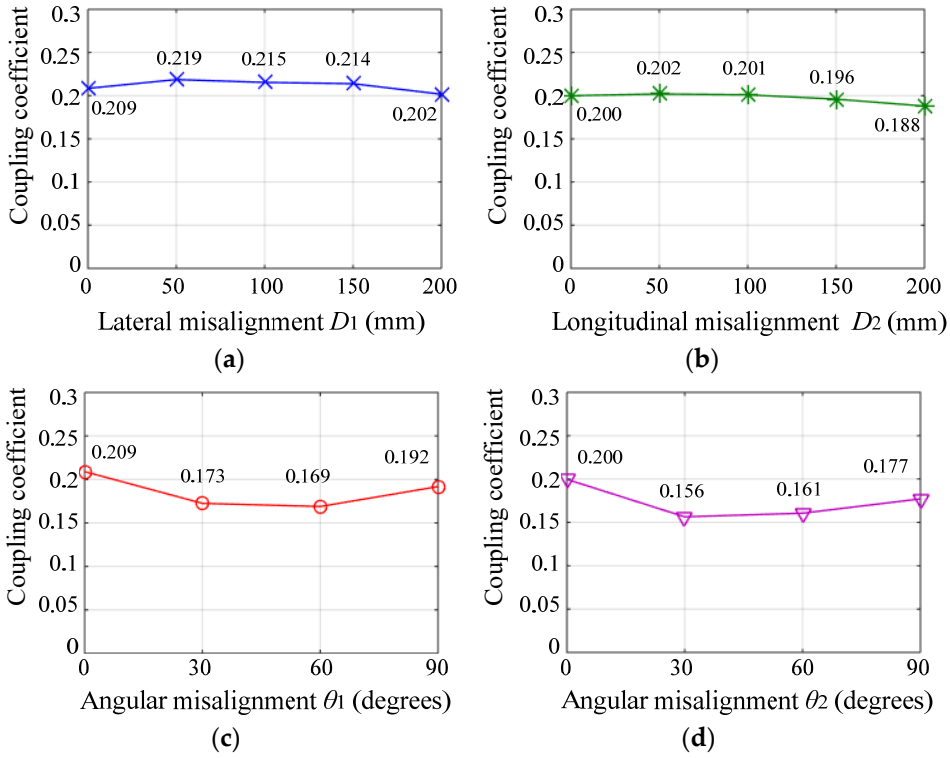

Figure 13. Measured coupling coefficient between the transmitter and receiver coils with (**a**) lateral coil misalignment D_1; (**b**) longitudinal coil misalignment D_2; (**c**) angular coil misalignment θ_1; (**d**) angular coil misalignment θ_2.

5.2. Measurement of the Load Powers and PGs

An experimental STMR-WPT system was constructed to verify the proposed single-frequency power allocation method, as shown in Figure 14a. The system mainly included a single-frequency power supply, a cross-overlapped bipolar transmitter coil, a switch, three square unipolar receiver coils, three loads and multiple C-CLCs networks.

The single-frequency power supply consisted of a signal generator FeelElec FY6900 and a high frequency power amplifier. The signal generator outputs a sine-wave signal with a frequency of 500 kHz, which is amplified by the power amplifier and then input into the transmitter circuit. The internal resistance of the power amplifier is 50 Ω.

The receiver coils were placed above the transmitter coil, as shown in Figure 14a, where the receiver coil-1 is aligned with the transmitter coil, the receiver coil-2 has a lateral misalignment of 50 mm, and the receiver coil-3 has an angular misalignment of 90 degrees. The measured inductances of the receiver coil-1, coil-2 and coil-3 were 44.1 μH, 44.5 μH and 44.3 μH, respectively. The measured mutual inductances between the transmitter coil and the receiver coil-1, coil-2 and coil-3 were 11.30 μH, 11.68 μH and 10.51 μH, respectively.

In order to simulate different load conditions, three thick film resistors with different resistance values were used as the loads of the STMR-WPT system, as marked in Load-1, Load-2, and Load-3 in Figure 14a. Their resistance values were 10, 50 and 100 Ω, as shown in Figure 14b.

The C-CLCs networks are made of variable capacitors and inductors, as shown in Figure 14c. In the experiment, four different power allocation scenarios were considered, including scenario-1 ($\gamma_b = 1.5$ and $\gamma_c = 3$), scenario-2 ($\gamma_b = \gamma_c = 1$), scenario-3 ($\gamma_b = 0.5$ and $\gamma_c = 100$) and scenario-4 ($\gamma_b = 100$ and $\gamma_c = 100$). Based on the proposed power allocation method, the optimal values of the C-CLCs networks in different scenarios

were calculated first. The results are listed in Table 5. Then, the variable capacitors and inductors in the C-CLCs networks were adjusted according to Table 5.

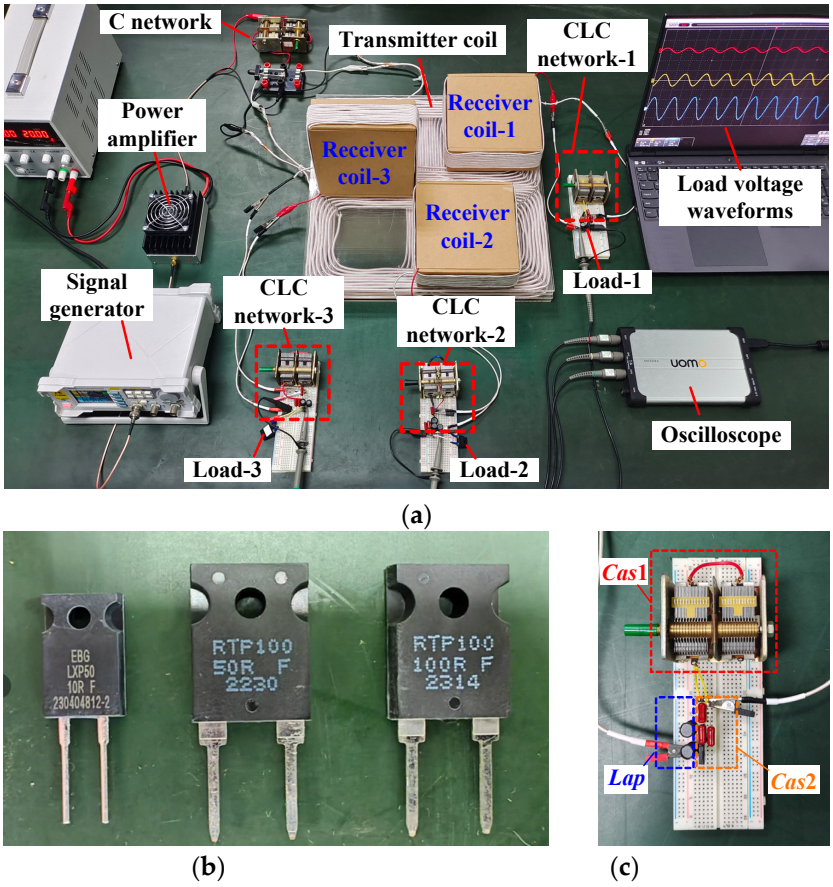

Figure 14. Hardware implementation of the STMR-WPT system. (**a**) Overall experimental system; (**b**) Thick film resistors; (**c**) CLC network-1.

Table 5. Values of the C-CLCs Networks in the Experiment.

Parameters	Scenario 1	Scenario 2	Scenario 3	Scenario 4
C_{ts}(nF)	1.5	1.5	1.5	1.5
L_{ap}(μH)	7.1	8.8	8.8	5.1
L_{bp}(μH)	20.2	20.2	14.3	118.0
L_{cp}(μH)	36.4	25.7	257.9	150.1
C_{as1}(nF)	2.0	1.9	1.9	2.1
C_{bs1}(nF)	1.6	1.6	1.7	0.6
C_{cs1}(nF)	1.3	1.4	0.3	0.5
C_{as2}(nF)	14.2	11.6	11.6	19.9
C_{bs2}(nF)	5.0	5.0	7.1	0.9
C_{cs2}(nF)	2.8	3.9	0.4	0.7

The maximum output power of the power amplifier was set to 30 W. An oscilloscope was used to measure the load voltages of the STMR-WPT system. Figure 15a–d, respectively, show the measured load voltage waveforms in scenario-1, scenario-2, scenario-3 and scenario-4. It can be seen that the RMS values of the load voltages in scenario-1 are: U_{La} = 11.3 V, U_{Lb} = 20.9 V and U_{Lc} = 21.3 V; the RMS values of the load voltages in scenario-2 are: U_{La} = 9.9 V, U_{Lb} = 20.7 V and U_{Lc} = 29.0 V; the RMS values of the load voltages in

scenario-3 are: U_{La} = 9.5 V, U_{Lb} = 28.9 V and U_{Lc} = 3.1 V; and the RMS values of the load voltages in scenario-4 are: U_{La} = 16.0 V, U_{Lb} = 3.8 V and U_{Lc} = 5.4 V.

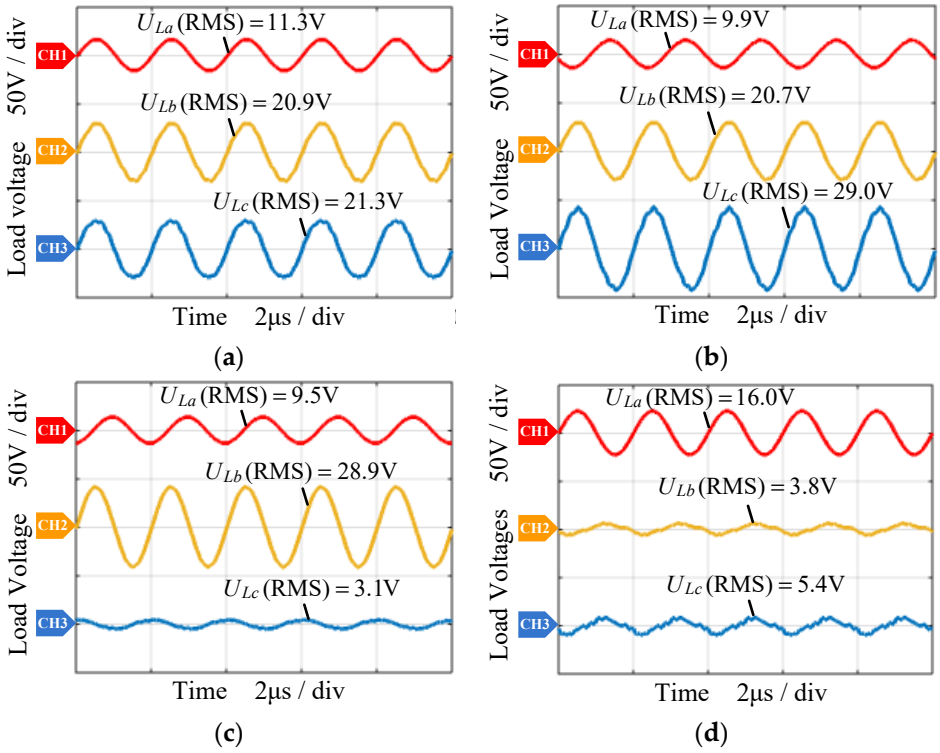

Figure 15. Measured load voltage waveforms in (**a**) scenario-1; (**b**) scenario-2; (**c**) scenario-3; (**d**) scenario-4.

Then, the load powers were calculated by:

$$P_L = \frac{{U_L}^2}{R_L} \tag{20}$$

where P_L is the load power, U_L is the RMS value of the load voltage, and R_L is the load resistance.

Figure 16a–d, respectively, show the load power distributions in scenarios-1, scenarios-2, scenarios-3 and scenarios-4. From Figure 16a, it can be seen that in scenario-1, the load powers of receiver-1, receiver-2 and receiver-3 are P_{La} = 12.8 W, P_{Lb} = 8.7 W and P_{Lc} = 4.5 W. The ratios of the load powers are P_{La} = 1.47P_{Lb} = 2.84P_{Lc}. It can be observed from Figure 16b that in scenario-2, the load powers are P_{La} = 9.8 W, P_{Lb} = 8.6 W and P_{Lc} = 8.4 W. The ratios of the load powers are P_{La} = 1.14P_{Lb} = 1.17P_{Lc}. Therefore, the three receivers obtain approximately the same load power in scenario-2.

It can be seen that from Figure 16c in scenario-3, the load powers are P_{La} = 9.0 W, P_{Lb} = 16.7 W and P_{Lc} = 0.1 W. The ratios of the load powers are P_{La} = 0.54P_{Lb} = 90.0P_{Lc}. Figure 16d shows that in scenario-4, the load powers are P_{La} = 25.6 W, P_{Lb} = 0.3 W and P_{Lc} = 0.3 W. The ratios of the load powers are P_{La} = 85.3P_{Lb} = 85.3P_{Lc}. Thus, most of the source output power is transmitted to receiver-1 in scenario-4.

From Figure 16, it can be obtained that the total load power P_{total} = P_{La} + P_{Lb} + P_{Lc} in scenario-1, scenario-2, scenario-3 and scenario-4 is 26.0 W, 26.8 W, 25.8 W and 26.2 W, respectively. Because the maximum output power of the power amplifier is 30 W, the total PG of the STMR-WPT system in scenario-1, scenario-2, scenario-3 and scenario-4 is 0.87, 0.89, 0.86 and 0.87, respectively. The measured output power of the power amplifier in scenario-1, scenario-2, scenario-3 and scenario-4 is 29.5, 29.7, 29.6 and 29.5 W, respectively.

Therefore, the PTE of the STMR-WPT system in scenario-1, scenario-2, scenario-3 and scenario-4 is 0.88, 0.90, 0.87 and 0.89, respectively.

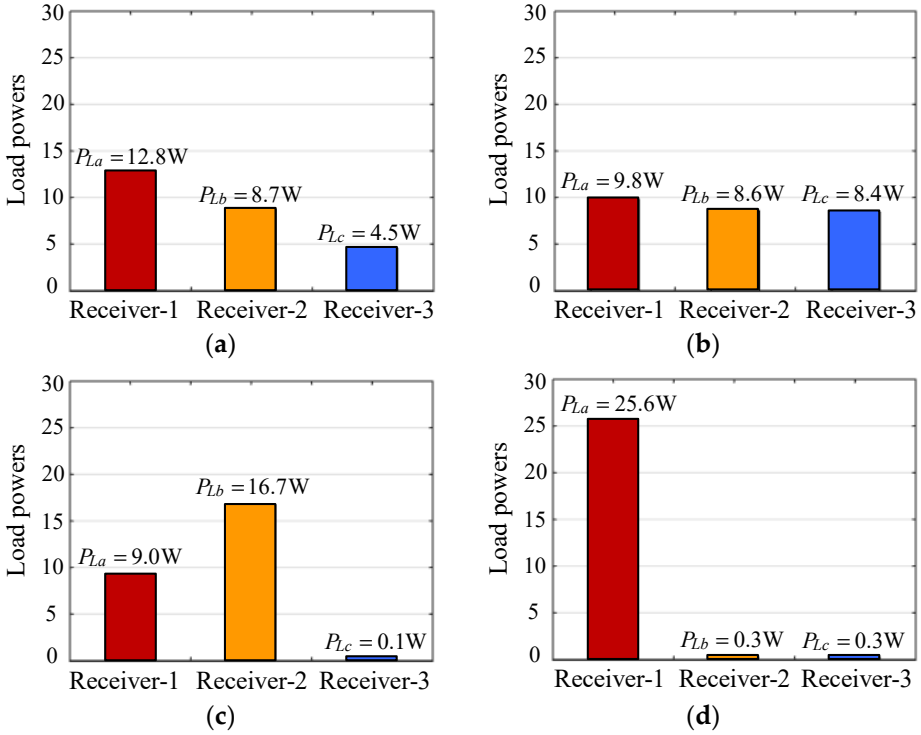

Figure 16. Measured load powers in (**a**) scenario-1; (**b**) scenario-2; (**c**) scenario-3; (**d**) scenario-4.

The experimental results show that the STMR-WPT system successfully achieves the expected power allocation goals and obtains high total PGs and PTEs in all four scenarios. The error between the target load power ratios and the measured load power ratios is mainly caused by factors such as the limited accuracy of the variable capacitors and inductors in the C-CLCs networks, and the voltage measurement error of the oscilloscope. In addition, the power losses of the capacitors and inductors are ignored in theoretical analysis. However, in the experiment, these circuit components also consumed some of the source power, which affected the measured values of the load power ratios.

For the convenience of the experimental operation, the size of the transmitter coil was designed to be 400 mm, the side length of the receiver coil was designed to be 160 mm, and the maximum output power of the power amplifier was set to 30 W. It should be pointed out that when the size of the transmitter and receiver coils change proportionally and the output power of the power amplifier varies within a reasonable range, the proposed coupling coil structure and power allocation method are still feasible.

The comparison between the previous STMR-WPT systems and the STMR-WPT system proposed in this article is shown in Table 6. It can be seen that the proposed STMR-WPT system has good tolerance for lateral, longitudinal and angular coil misalignments. Moreover, in the proposed STMR-WPT system, the C-CLCs networks are constructed to achieve separate load power allocation for the receivers. Thus, relay coils, complex multi-frequency transmission channels and independent power supplies with different frequencies can be avoided, which is beneficial for reducing the system size and cost. By using the proposed power allocation method, the STMR-WPT system can operate in single-frequency mode and achieve load power allocation at any specified ratios under different mutual inductance and load impedance conditions.

Table 6. Comparison with Previous STMR-WPT Systems with Load Power Allocation Function.

Reference	Number of Receiver Coils in the Experiment	Structure of the Magnetic Coupling Coils	Tolerance for Coil Misalignments	Using Relay Coils	Using Multi-Frequency Transmission Channels	Requirement for the Power Supply	Load Power Allocation Ratios
[20]	4	Planar-spiral coils	Sensitive	Yes	No	A single-frequency power supply	Fixed
[23]	2, 3 and 4	Solenoid coils	Sensitive	Yes	Yes	A multi-frequency power supply	Variable
[25]	2	Planar-spiral coils	Sensitive	No	Yes	Multiple power supplies	Variable
[26]	2	Solenoid coils	Sensitive	No	Yes	A multi-frequency power supply	Variable
[30]	2	3D solenoid coils	Good tolerance for lateral coil misalignment	No	No	A single-frequency power supply	Fixed
[31]	2	3D orthogonal omnidirectional coils	Good tolerance for angular coil misalignment	No	No	Multiple power supplies	Variable
This article	3	Cross-overlapped bipolar transmitter coil and square receiver coil	Good tolerance for lateral, longitudinal and angular coil misalignments	No	No	A single-frequency power supply	Any specified power allocation ratios

6. Discussion

The cross-overlapped bipolar transmitter coil proposed in this article has a similar appearance to the four-pole transmitter coil shown in Figure 17, but their structure and function are different. The four-pole coil can save one switch, but it has some limitations: Firstly, if the transmitter and receiver coils are parallel and the receiver coil is placed at the boundary of two square coils, as shown in Figure 17, the coupling coefficient between the four-pole transmitter coil and the receiver coil is very low. Secondly, in the four-pole transmitter coil shown in Figure 17, the four small square coils can only be activated or deactivated simultaneously, which may increase the leakage flux of the system.

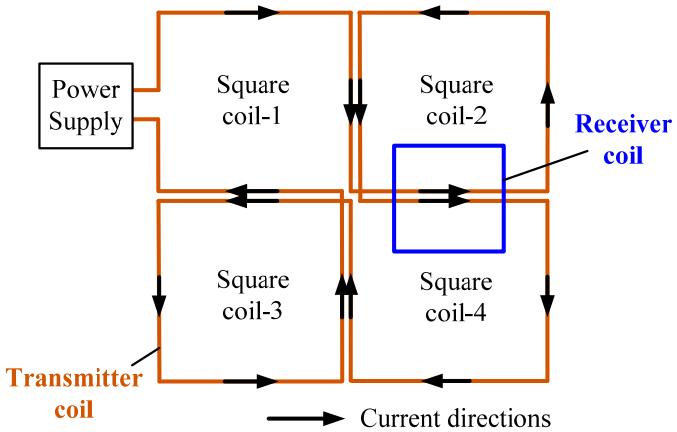

Figure 17. Structure of the four-pole square coil.

Compared with the four-pole transmitter coil, the cross-overlapped bipolar transmitter coil proposed in this article can overcome the above limitations. Even if the receiver coil is placed at the boundary of two square coils, the coupling coefficient between the transmitter

and receiver coils can remain stable by changing the switch state, as demonstrated by the experimental results in Figure 13. Moreover, in the proposed cross-overlapped bipolar transmitter coil, only one bipolar coil is activated at the same time, which is beneficial for reducing leakage flux and increasing the system efficiency. In practical applications, since there are only two switch states, the load power of the receiver can be measured in both switch states before starting wireless charging. The switch state that allows the receiver to obtain the desired load power can be activated.

In this article, the receiver coils were placed in positions where they were decoupled from each other. In practical applications, the receiver coil is usually not an independent module but is integrated inside a terminal equipment. Due to the limitations of the structure and volume of the terminal equipment, multiple receiver coils are often far away or decoupled from each other. The mutual influence between them can be ignored. However, in some special applications, the receiver coils may overlap with each other, resulting in a high coupling coefficient between them. The influence of mutual inductance between the receiver coils on the STMR-WPT system deserves further investigation in future research.

For the convenience of conducting experimental research, the experimental STMR-WPT system was constructed using separate components in this article. In the next step of research, the transmitter and receiver coils, C-CLCs networks, and other circuit components can be integrated on the PCB to reduce the volume of the STMR-WPT system and improve its reliability.

7. Conclusions

In order to overcome the limitations of traditional STMR-WPT systems, this article proposes a STMR-WPT system in which a cross-overlapped bipolar coil is used as the transmitter, and multiple square unipolar coils are employed as the receivers. By using this structure, the magnetic field of the system can be adjusted to accommodate different coil misalignment conditions. Then, a single-frequency power allocation method is presented, which allows the STMR-WPT system to achieve separate load power allocation without using relay coils, multi-frequency transmission channels, or independent power supplies with different frequencies. Finally, an experimental system is established to verify the proposed method. The experimental results show that when the lateral or longitudinal coil misalignment varies within the range of 0~200 mm, the coupling coefficient decreases by a maximum of 6% compared to the initial value, and when the angular coil misalignment varies within the range of 0~90 degrees, the coupling coefficient decreases by a maximum of 22% compared to the initial value. By using the proposed power allocation method, the STMR-WPT system can achieve load power allocation at any specified ratios under different mutual inductance and load impedance conditions. Meanwhile, the total PG of the system can be maximized. The STMR-WPT system proposed in this article has good application prospects in scenarios where multiple load devices with different power requirements need to be charged simultaneously.

Author Contributions: Conceptualization, Y.L. and Y.Y.; methodology, Y.L.; validation, Y.L. and Z.D.; formal analysis, Y.L. and Z.D.; investigation, Z.D.; writing—original draft preparation, Y.L.; writing—review and editing, Y.Y. and Z.D. All authors have read and agreed to the published version of the manuscript.

Funding: This work was supported by the National Natural Science Foundation of China under Grant 52107013.

Data Availability Statement: Data are contained within the article.

Conflicts of Interest: The authors declare no conflicts of interest.

References

1. Li, Y.; Zhang, B.; Zhai, Y.; Wang, H.; Yuan, B.; Lou, Z. A Novel Type of 3-D Transmitter for Omnidirectional Wireless Power Transfer. *IEEE Trans. Power Electron.* **2024**, *39*, 6537–6548. [CrossRef]

2. Yan, Z.; Wu, M.; Zhao, C.; Hu, Q.; Zhu, L.; Qiao, L.; Wang, L. Free-Rotation Wireless Power Transfer System Based on Composite Anti-Misalignment Method for AUVs. *IEEE Trans. Power Electron.* **2023**, *38*, 4262–4266. [CrossRef]
3. Yue, K.; Liu, Y.; Zhang, X.; Fu, M.; Liang, J.; Wang, H. Transmitter-Side Voltage-Based Mutual Inductances and Load Tracking for Two-Transmitter LCC-S Compensated Wireless Power Transfer Systems. *IEEE J. Emerg. Sel. Top. Power Electron.* **2024**, *12*, 2317–2332. [CrossRef]
4. Li, X.; Zheng, F.; Wang, H.; Sun, Y.; Dai, X.; Hu, J. A Simultaneous Power and Data Transfer Method for Dynamic Wireless Charging Electric Vehicles. *IEEE J. Emerg. Sel. Top. Power Electron.* **2024**, *12*, 328–340. [CrossRef]
5. Zeng, Y.; Lu, C.; Liu, R.; He, X.; Rong, C.; Liu, M. Wireless Power and Data Transfer System Using Multidirectional Magnetic Coupler for Swarm AUVs. *IEEE Trans. Power Electron.* **2023**, *38*, 1440–1444. [CrossRef]
6. Li, M.; Khaleghi, A.; Hasanvand, A.; Narayanan, R.P.; Balasingham, I. A New Design and Analysis for Metasurface-Based Near-Field Magnetic Wireless Power Transfer for Deep Implants. *IEEE Trans. Power Electron.* **2024**, *39*, 6442–6454. [CrossRef]
7. Xiong, W.; Jiang, F.; Liu, Z.; Zhu, Q.; Su, M. A Hybrid-Frequency-Based Multi-Load Wireless Power Transfer System with Constant Current or Voltage Outputs. *IEEE J. Emerg. Sel. Top. Power Electron.* **2024**, *12*, 1150–1160. [CrossRef]
8. Pang, H.; Chau, K.T.; Liu, W.; Tian, X. Multi-Resonating Compensation for Multi-Channel Multi-Pickup Wireless Power Transfer. *IEEE Trans. Magn.* **2022**, *58*, 8600506. [CrossRef]
9. Lee, S.B.; Jang, I.G. Coil Layout Optimization for Maximizing the Power Transfer Efficiency of Wireless Power Transfer Systems with Multiple Transmitter Coils. *IEEE J. Emerg. Sel. Top. Power Electron.* **2020**, *8*, 2672–2681. [CrossRef]
10. Jeon, S.-J.; Seo, D.-W. Effect of Additional Transmitting Coils on Transfer Distance in Multiple-Transmitter Wireless Power Transfer System. *IEEE Access* **2022**, *10*, 9174–9183. [CrossRef]
11. Pathmanathan, M.; Nie, S.; Yakop, N.; Lehn, P.W. Space-Vector Based Excitation of a Bipolar Transmitter for Wireless Power Transfer Applications. *IEEE Trans. Ind. Electron.* **2021**, *68*, 12524–12534. [CrossRef]
12. Han, W.; Chau, K.T.; Hua, Z.; Pang, H. Compact Wireless Motor Drive Using Orthogonal Bipolar Coils for Coordinated Operation of Robotic Arms. *IEEE Trans. Magn.* **2022**, *58*, 8200608. [CrossRef]
13. Zhu, Y.; Zhang, H.; Wang, Z.; Cao, X.; Zhang, R. Design of a high-power high-efficiency multi-receiver wireless power transfer system. *Electronics* **2021**, *10*, 1308. [CrossRef]
14. Zhou, L.; Liu, S.; Li, Y.; Mai, R.; Li, Y.; Fu, L.; Qi, L. Efficiency Optimization of LCC-S Compensated Multiple-Receiver Bidirectional WPT System for Stackers in Automated Storage and Retrieval Systems. *IEEE Trans. Power Electron.* **2022**, *37*, 15693–15705. [CrossRef]
15. Fu, M.; Yin, H.; Liu, M.; Wang, Y.; Ma, C. A 6.78 MHz Multiple-Receiver Wireless Power Transfer System with Constant Output Voltage and Optimum Efficiency. *IEEE Trans. Power Electron.* **2018**, *33*, 5330–5340. [CrossRef]
16. Kobuchi, D.; Matsuura, K.; Narusue, Y.; Morikawa, H. Magnetic Field Leakage Cancellation in Multiple-Input Multiple-Output Wireless Power Transfer Systems. *IEEE Magn. Lett.* **2022**, *13*, 1–4. [CrossRef]
17. Li, J.; Lin, J.-K.; Song, X.; Yan, S.; Xu, K.-D.; Zhang, X.Y. Efficiency-Enhanced Wireless Power Transfer Based on Multiple Coupling Paths. *IEEE Microw. Wirel. Compon. Lett.* **2022**, *32*, 444–447. [CrossRef]
18. Cheng, C.; Lu, F.; Zhou, Z.; Li, W.; Deng, Z.; Li, F.; Mi, C. A Load-Independent LCC-Compensated Wireless Power Transfer System for Multiple Loads with a Compact Coupler Design. *IEEE Trans. Ind. Electron.* **2020**, *67*, 4507–4515. [CrossRef]
19. Ishihara, M.; Fujiki, K.; Umetani, K.; Hiraki, E. Autonomous System Concept of Multiple-Receiver Inductive Coupling Wireless Power Transfer for Output Power Stabilization Against Cross-Interference Among Receivers and Resonance Frequency Tolerance. *IEEE Trans. Ind. Appl.* **2021**, *57*, 3898–3910. [CrossRef]
20. Ji, X.; Zhao, P.; Wang, H.; Yang, H.; Fu, M. Multiple-Receiver Inductive Power Transfer System Based on Multiple-Coil Power Relay Module. *IEEE Trans. Circuits-I* **2023**, *70*, 2625–2634. [CrossRef]
21. Cho, J.-H.; Jung, S.; Kim, Y.-J. Wireless Power Transfer for Variable Load, Distance, and Power Division Ratio in a Loosely-Coupled Multiple-Receiver Relay System. *IEEE Trans. Ind. Electron.* **2023**, *70*, 6809–6818. [CrossRef]
22. Lee, K.; Choi, H.-H. Fast Wireless Power Transfer for Multiple Receivers in Linear Topology. *IEEE Syst. J.* **2020**, *14*, 649–652. [CrossRef]
23. Narayanamoorthi, R.; Vimala Juliet, A.; Chokkalingam, B. Cross Interference Minimization and Simultaneous Wireless Power Transfer to Multiple Frequency Loads Using Frequency Bifurcation Approach. *IEEE Trans. Power Electron.* **2019**, *34*, 10898–10909. [CrossRef]
24. Gao, X.; Du, B.; Zhang, Y.; Cui, S. A Dual-Frequency Compatible Wireless Power Transfer System with a Single Transmitter and Multiple Receivers. *IEEE Access* **2022**, *10*, 102564–102574. [CrossRef]
25. Huang, Y.; Liu, C.; Xiao, Y.; Liu, S. Separate Power Allocation and Control Method Based on Multiple Power Channels for Wireless Power Transfer. *IEEE Trans. Power Electron.* **2020**, *35*, 9046–9056. [CrossRef]
26. Tian, X.; Chau, K.T.; Pang, H.; Liu, W. Power Adaption Design for Multifrequency Wireless Power Transfer System. *IEEE Trans. Magn.* **2022**, *58*, 1–5. [CrossRef]
27. Xiao, Y.; Liu, C.; Huang, Y.; Liu, S. Concurrent Wireless Power Transfer to Multiple Receivers with Additional Resonant Frequencies and Reduced Power Switches. *IEEE Trans. Ind. Electron.* **2020**, *67*, 9292–9301. [CrossRef]
28. Liu, Y.; Liu, C.; Huang, R.; Song, Z. Primary Multi-Frequency Constant-Current Compensation for One-to-Multiple Wireless Power Transfer. *IEEE Trans. Circuit-II* **2023**, *70*, 2201–2205. [CrossRef]

29. Wu, S.; Cai, C.; Liu, X.; Chai, W.; Yang, S. Compact and Free-Positioning Omnidirectional Wireless Power Transfer System for Unmanned Aerial Vehicle Charging Applications. *IEEE Trans. Power Electron.* **2022**, *37*, 8790–8794. [CrossRef]
30. Pahlavan, S.; Jafarabadi-Ashtiani, S.; Mirbozorgi, S.A. Maze-Based Scalable Wireless Power Transmission Experimental Arena for Freely Moving Small Animals Applications. *IEEE Trans. Biomed. Circ. Sys.* **2024**, *99*, 99. [CrossRef]
31. Pahlavan, S.; Shooshtari, M.; Jafarabadi Ashtiani, S. Star-Shaped Coils in the Transmitter Array for Receiver Rotation Tolerance in Free-Moving Wireless Power Transfer Applications. *Energies* **2022**, *15*, 8643. [CrossRef]
32. Zhang, C.; Lu, W.; Zhao, J.; Wu, X.; Chen, H.; Xu, D. A Novel Asymmetric Magnetic Coupler Applied to Multiple-Receiver Wireless Charging System for Automated Guided Vehicles. *IEEE Trans. Power Electron.* **2023**, *38*, 14761–14775. [CrossRef]
33. Zhu, Z.; Yang, A.; Yuan, H.; Zhao, C.; Chen, F.; Wang, X.; Rong, M. Efficiency Optimization and Power Allocation of Omnidirectional Wireless Power Transfer for Multiple Receivers. *IEEE Trans. Ind. Electron.* **2023**, *70*, 9689–9699. [CrossRef]
34. Kim, S.-Y.; Kwon, N.-R.; Ahn, S.-H.; Lee, W.-S. Three-Dimensional Wireless Power Transfer System Using Multiple Orthogonal Resonators for Spatial Freedom. *IEEE Trans. Antenn. Propag.* **2023**, *71*, 4036–4044. [CrossRef]